Flow Tube Studies of Benzene Charge Transfer Reactions from 250 to 1400 K

Susan T. Arnold,[†] Skip Williams, Itzhak Dotan,[‡] Anthony J. Midey, Robert A. Morris, and A. A. Viggiano*

Air Force Research Laboratory, Space Vehicles Directorate, 29 Randolph Road, Hanscom AFB, Massachusetts 01731-3010

Received: June 11, 1999; In Final Form: August 23, 1999

Temperature dependent rate constants and product branching fractions are reported for reactions of the atmospheric plasma cations NO^+, O_2^+, O^+, N^+, N_2^+, and N_4^+ with benzene, as measured from 250 to 500 K by the selected ion flow tube technique. For the reactions of O_2^+ and N_2^+, data have also been obtained between 500 and 1400 K in a high-temperature flowing afterglow. These are among the first determinations of ion−molecule branching fractions above 600 K. Temperature dependent rate constants and product branching fractions are also reported for the reactions of benzene with Kr^+, Ar^+, Ne^+, and F^+. All reactions were found to proceed at the collision rate at all temperatures studied. With increasing reactant ion recombination energy, the mechanism changed from association and nondissociative charge transfer to dissociative charge transfer. Primary and secondary dissociation products were observed. Some of the reactivity in the N^+ and F^+ reactions is attributed to chemical channels. The temperature dependent branching fractions are converted to product ion breakdown curves and compared to previous studies. The current results exhibit a kinetic shift, resulting from slow fragmentation of the $C_6H_6^{+}$* complex, combined with collisional stabilization of the complex by the He buffer gas. The pressure dependence of the N^+ reaction was examined from 0.35 to 0.8 Torr. The flow tube data provide the first breakdown curve for the $C_5H_3^+$ product and further indicate that $C_5H_3^+$ is relatively unreactive, consistent with it having the cyclic ethynyl cyclopropene ion structure. The $C_3H_3^+$ product was shown to have a cyclic structure, while the $C_4H_4^+$ product was found to be a mixture of linear and cyclic isomers. The isomeric mixture of $C_4H_4^+$ products was quantified as a function of the $C_6H_6^{+}$* excess energy. A schematic reaction coordinate diagram representing the primary dissociation channels of $C_6H_6^+$ is constructed from previous experimental and theoretical work. A possible reaction pathway for the $C_5H_3^+$ product is discussed.

Introduction

In the 1960s, Jonsson and Lindolm[1] utilized the technique of charge exchange mass spectrometry to develop a breakdown diagram for benzene. These results were later refined by Eland et al.[2] using the photoelectron−photoion coincidence technique. Over the years, the dissociation of benzene cation has received much experimental and theoretical attention, and a clear picture of the dissociation has now emerged. Briefly, there are at least four primary dissociation product channels competing at threshold ($C_6H_5^+$, $C_6H_4^+$, $C_4H_4^+$, and $C_3H_3^+$), and the dissociation is well described by statistical theories. For a more thorough discussion of the benzene cation dissociation, the reader is directed to the review by Rosenstock et al.[3]

We have undertaken the current study of benzene charge transfer reactions as a continuation of our program to explore the potential enhancing effects of ionization on hydrocarbon combustion and ignition processes. Such effects have been noted in aeronautical engineering experiments but have not been explained. Previously, we have examined reactions of atmospheric plasma ions with a series of normal and branched alkanes for species up to dodecane.[4−6] These investigations showed generally a high degree of reactivity and numerous product channels involving alkane fragmentation. The fast reaction rates, dissociative pathways, and production of free radical species led us to speculate that these reactions might have an impact on alkane ignition and/or combustion in the presence of ionized air. Preliminary combustion kinetics modeling results have supported this speculation in the case of isooctane ignition, indicating a decrease in ignition delay time with increasing levels of ionization.[7] To extend the kinetics database and allow the continued examination of the effects of ionization on hydrocarbon combustion processes, we have undertaken a series of kinetics measurements of aromatic compounds. In this paper, we report temperature dependent rate constants and product branching fractions for the reactions of the atmospheric plasma cations NO^+, O_2^+, O^+, N^+, N_2^+, and N_4^+ with benzene, as measured from 250 to 500 K by the selected ion flow tube technique. For the reactions of O_2^+ and N_2^+, we also report measurements from a high temperature flowing afterglow apparatus that extend the kinetics results to 1400 K. Along with our recent reports of naphthalene charge transfer reactions[8] and methane reaction with O_2^+,[9] this study represents the first time product branching fractions for ion−molecule reactions have been recorded at such high temperatures.

In addition to studying the reactions of atmospheric plasma ions with benzene, we also report temperature dependent rate constants and product branching fractions for the reactions of benzene with Kr^+, Ar^+, Ne^+, and F^+. These reactants are

[†] Under contract to Aerodyne Research, Billerica, MA.

[‡] NRC Senior Research Fellow. Permanent address: Department of Natural and Life Sciences, The Open University of Israel, 16 Klausner St. Ramat-Aviv, Tel-Aviv, Israel.

10.1021/jp991928k CCC: $18.00
Published on Web 09/30/1999

included, so product ion breakdown curves can be constructed from the flow tube data, as recently demonstrated by Praxmarer et al.[10] This allows for a direct comparison to be made between the flow tube data and data obtained under lower pressure conditions.

Experimental Section

Measurements of various cations reacting with C_6H_6 from 250 to 500 K were made using the Air Force Research Laboratory's (AFRL) variable temperature selected ion flow tube (VT-SIFT). Additional measurements of O_2^+ and N_2^+ reactions with C_6H_6 from 500 to 1400 K were made using the AFRL's high temperature flowing afterglow (HTFA). Both instruments have been described previously in detail,[11,12] and only brief descriptions of each method and details pertinent to the present study are given here.

VT-SIFT (250−500 K). Reactant ions were produced in a moderate pressure ion source (0.1−1 Torr) by electron impact on a precursor compound: NO for NO^+; O_2 for O^+ and O_2^+; N_2 for N^+ and N_2^+; Ar for Ar^+; Kr for Kr^+; Ne for Ne^+; and SF_6 for F^+. The reactant ion of interest was mass selected in a quadrupole mass filter and injected into the flow tube through a Venturi inlet into a fast flow of He buffer gas ($\sim$100 m s^{-1}). The buffer gas (He, 99.997%) was passed through a molecular sieve/liquid nitrogen trap to reduce residual water vapor. Generally, the flow tube was maintained at a total pressure of $\sim$ 0.45 Torr, although the pressure was varied from 0.3 to 1.0 Torr for several experiments. For the N_4^+ experiments, reactant ions were formed in the upstream end of the flow tube, prior to reaction with C_6H_6, by injecting N_2^+ into the flow tube and reacting to completion with N_2. The benzene reactant was obtained commercially (Mallinckrodt, 99%) and used without further purification except for repeated freeze−pump−thaw cycles to eliminate dissolved gases. The reactant was introduced downstream through a finger inlet, 1/8 in. tubing entering the flow tube perpendicular to the flow and terminating at the radial center of the tube. The reaction time was determined from previous time-of-flight measurements. A small fraction of the gas in the tube flowed through a sampling orifice, and the reactant and product ions in this flow were mass analyzed in a second quadrupole mass filter and detected by a particle multiplier. Rate constants were extracted from least-squares fits of the plots of the logarithm of the reactant ion signal versus the concentration of the reactant neutral. The accuracy of the measured overall rate constants is ±25%, while the relative accuracy is ±15%.[11]

Product branching fractions were determined by recording the product ion count rates as a function of the reactant neutral flow rate. To account for the effects of secondary reactions between the product ions and the reactant neutral, the reported branching fractions were determined by extrapolating the measured values to a neutral reactant flow rate of zero. Branching fractions were obtained by operating the mass spectrometer at two different resolution settings. A higher resolution setting was used to determine the branching ratio between product ions of similar mass (those differing by one or two hydrogen atoms), and this ratio was applied to lower resolution data taken to minimize mass discrimination wherein the species of similar mass appeared as a single broad peak. In determining the product branching fractions, it was necessary to account for significant ^{13}C isotopic products. Comparing the reactant ion signal loss to the sum of the product ion signals yields a maximum absolute uncertainty in the branching fractions of 25%. The relative error between the branching fractions of any given product ion and the major product is 10%.

The formation of electronically excited NO^+ and O^+ reactant ions was monitored by introducing a small flow of N_2 into the SIFT, prior to introducing the benzene. Only the excited electronic states of NO^+ and O^+ charge transfer with N_2,[13] so it was possible to monitor the formation of N_2^+ and then vary source conditions until less than 2% of the reactant ions were being formed as NO^+* and O^+*. Similarly, the formation of N^+* was monitored using D_2; the ground state reaction yields exclusively ND^+, while the reaction of metastable N^+ yields exclusively D_2^+.[14] The formation of F^+* was not monitored since there are no relatively low lying excited electronic states.[15] Vibrationally excited states of NO^+, O_2^+, and N_2^+ were quenched prior to reaction by introducing a flow of N_2 into the tube upstream of the reaction zone.[16] The reactivity of the two Kr^+ spin−orbit states was distinguished by examining the reaction of Kr^+ formed by direct electron impact to the reaction of Kr^+ formed by fragmentation of Kr_2^+. The former method produces a statistical mixture of spin states, and the latter method produces only the lower spin−orbit state.[11]

HTFA (500−1400 K). A commercial furnace heated the quartz flow tube to the desired temperature. Helium buffer gas (99.997%) was introduced into the upstream end of the flow tube after first passing through a molecular sieve/liquid nitrogen trap to reduce residual water vapor. The pressure of the flow tube was maintained at 0.6 to 1.2 Torr. Metastable He ($2\ ^3S$) atoms and He^+ ions were formed at the upstream end of the flow tube by electron impact, and reaction of He* and He^+ with a neutral precursor gas, introduced just downstream of the filament, generated the reactant ions of interest via Penning ionization and charge transfer. The O_2^+ and N_2^+ reactants were generated from O_2 and N_2, respectively. Using relatively large flows of O_2 and N_2 ensured that all He*, O^+, and excited O_2^+ and N_2^+ were consumed prior to the reaction zone. However, in the N_2^+ experiments, the use of large N_2 flows also resulted in the formation of N_4^+. This complication is addressed below in more detail. For the N_2^+ experiments, it was also necessary to use low electron energies in order to reduce the formation of N^+ formed by reaction of N_2 and He^+. The reactant ions were carried downstream by the buffer gas, allowed to thermally equilibrate, and then were reacted with C_6H_6 vapor. Reaction times were determined by previous time-of-flight measurements. A small fraction of the gas in the tube flowed through a sampling orifice, and the reactant and product ions in this flow were mass analyzed in a quadrupole mass filter and detected by a particle multiplier. As in the VT-SIFT measurements, rate constants were extracted from least-squares fits of the plots of the logarithm of the reactant ion signal versus the concentration of the reactant neutral. The accuracy of the measured overall rate constants is ±25%, and the relative accuracy is ±15%.[12]

A recent improvement in pumping efficiency on the vacuum box housing the furnace and flow tube now allows parent ions of simple molecules such as N_2 and O_2 to be produced with near 100% purity. The elimination of most impurities in the HTFA, especially water vapor, as well as several other experimental refinements, permits us to measure high temperature product branching fractions for reactions of simple ions. Branching fractions were determined as described above for the VT-SIFT, i.e., by recording the product ion count rates as a function of the neutral reactant flow rate and extrapolating the measured branching percentages to a neutral reactant flow rate of zero. Branching fractions were obtained by operating the mass spectrometer at two different resolution settings: a higher resolution setting to determine the branching ratio between

product ions of similar mass and a lower resolution setting to minimize mass discrimination.

The product branching data obtained in this manner were then corrected to account for products of other primary ions present simultaneously in the flow tube. In particular, the N_2^+ data required a correction for N_4^+. From the VT-SIFT experiments, it was shown that N_4^+ reacts at the collision rate with C_6H_6 to yield a single product ion, $C_6H_6^+$. This correction was most important at 500 K where N_4^+ was still formed readily; however, it became less significant by 800 K, and unimportant at higher temperatures. At temperatures above 800 K, another complication arose; namely, large signals of alkali ions were observed because the flow tube and/or sampling cone emit alkali metals at significant rates at these temperatures. The dominant ion observed was K^+, along with some Na^+ and small amounts of Rb^+. While benzene cannot undergo charge transfer with the alkali cations because their recombination energies are too low, their presence created a significant problem for the N_2^+ branching fraction determination because there was a mass coincidence between K^+ and one of the main reaction product ions, namely $C_3H_3^+$. By adjusting N_2 flow conditions so the formation of N_2^+ product ions was several times larger than the K^+ signal, it was possible to obtain an upper limit for the $C_3H_3^+$ branching fraction. Given these two complications, one significant below 800 K, the other significant above 800 K, the relative uncertainty in the reported branching fractions is estimated to be ±20%.

One final complication to consider is the potential pyrolysis of the benzene reactant at elevated temperatures. Previous mass spectrometric studies indicate that, over the pressure range of the present experiments, there is no pyrolysis up to 1100 K.[17] At 1400 K, the mass spectrometric studies indicate that approximately 10% of the benzene is pyrolyzed. In the 0.01−1 Torr pressure range, the major gas phase products are H, H_2, C_2H_2, and C_4H_2, as well as larger polycyclic aromatic hydrocarbons. Of course, this mass spectral value for the extent of benzene pyrolysis at high temperatures represents only an estimate, as pyrolysis of benzene in the HTFA will also likely depend on what other gaseous components are present in the flow tube, i.e., O_2 or N_2.

Results

Reaction rate constants and product branching fractions, measured with the VT-SIFT in the temperature range from 250 to 500 K, are shown in Table 1 for the reactions of benzene with NO^+, O_2^+, N_4^+, O^+, $Kr^+(^2P_{3/2})$, N^+, $Kr^+(^2P_{1/2})$, N_2^+, Ar^+, F^+, and Ne^+. The reported rates were determined from 2 to 20 replicate measurements. The reactant ions are listed in Table 1 in order of increasing recombination energy. An effective recombination energy of 12.9 eV was used for N_4^+, as suggested by Praxmarer et al.[10] Given that the ionization potential of benzene is 9.25 eV, this set of reactant ions allows us to study a series of benzene charge transfer reactions ranging from nearly thermoneutral (NO^+) to over 12 eV exothermic (Ne^+). For each reactant ion in Table 1, the detected ionic products are indicated along with the assumed neutral products. As discussed in more detail below, the neutral products for some reaction channels are shown in parentheses, indicating these are the assumed products based on energetics. Collisional rate constants are also indicated in Table 1.[18−20]

NO^+ Reactions. The reaction of NO^+ with benzene proceeds at the collision rate from 300 to 500 K and yields two product ions: charge transfer and association products. At 300 K, the branching fraction for the charge transfer product ion is 0.73, and it increases to 0.99 by 500 K as the association product channel nearly disappears. In a previous measurement of this reaction, Spanel and Smith[21] report a smaller branching fraction (0.15) for the association channel at 300 K. Because the association product bond is relatively weak, determination of the branching ratio is very sensitive to the flow tube sampling conditions, and this could explain the noted discrepancy. The discussion below on the temperature dependence of the reaction indicates good agreement with theory, supporting the present measurements.

The pressure dependence of this reaction was measured from 0.33 to 0.96 Torr at 300 K. The total rate constant was found to be independent of pressure within our relative uncertainty. In contrast, the branching fraction changed substantially with pressure. The rate constant for the association channel is shown in Figure 1a. Increasing pressure yields more of the association product but in a nonlinear manner. This indicates that the reaction is in the falloff region of association reactions. This is not surprising since the rate constant is approaching one-third of the collisional value.

We have also studied the temperature dependence of the three-body rate constant for the association channel at a fixed pressure of 0.45 Torr. The results are shown in Figure 1b. We have calculated the temperature dependence using a model strictly applicable to the low-pressure limit.[22] The dashed curve in Figure 1b represents this calculation normalized to the 300 K data point. Remarkably good agreement is found, especially considering that the low pressure assumption is not applicable. The model essentially represents the temperature dependence of the partition functions of the reactants. The curvature in the plot shows the increasing influence of the benzene vibrations. A complete pressure and temperature study is beyond the scope of the present work.

O_2^+, N_4^+, O^+, and $Kr^+(^2P_{3/2})$ Reactions. The reactions of O_2^+, N_4^+, O^+, and $Kr^+(^2P_{3/2})$ all proceed at the collision rate from 300 to 500 K, and the only product channel for each reactant is nondissociative charge transfer. A limit of >0.99 is reported for the $C_6H_6^+$ branching fraction for the N_4^+ reaction because of the possibility that a minor amount of N_2^+ remained in the tube prior to reaction with C_6H_6. The reaction of benzene with $Kr^+(^2P_{3/2})$ was measured by injecting Kr_2^+ into the flow tube, a fraction of which dissociates upon injection, giving exclusively $Kr^+(^2P_{3/2})$. Although some undissociated Kr_2^+ remained in the flow tube, we were able to determine that both $Kr^+(^2P_{3/2})$ and Kr_2^+ form only $C_6H_6^+$ products since no other product ions were detected. This is not a surprising result for Kr_2^+ since the effective recombination energy, as suggested by Praxmarer et al.,[10] is 11.9 eV, below even that of O_2^+ which is a reactant that yields only charge transfer product ions.

The temperature dependence of the O_2^+ reaction was further examined using the HTFA; reaction rate constants and product branching fractions measured from 500 to 1400 K are shown in Table 2. Also presented in this table is the total energy of the reactants at these elevated temperatures. The total energy includes the center-of-mass translational energy, rotational energy, and vibrational energy. The vibrational energy contribution, above the zero point energy, was calculated from standard statistical mechanics formulas, using vibrational frequencies tabulated by Herzberg.[23] At 500 K, there is good agreement between the HTFA and VT-SIFT data. As the temperature increases, the rate constants remain collisional and $C_4H_n^+$ and $C_6H_5^+$ products are observed in addition to the still dominant nondissociative charge-transfer product. At 1400 K, almost 10% of the products are ions other than $C_6H_6^+$. If these products are

TABLE 1: Temperature Dependent Bimolecular Rate Constants and Product Branching Fractions, as Measured with the VT-SIFT, for Reactions of Benzene with Various Ions[a]

		rate constant (10^{-9} cm^3 s^{-1}), (k_c), branching fractions				
reaction	ion RE (eV)	250 K	300 K	350 K	400 K	500 K
$NO^+ + C_6H_6 \rightarrow$ products	9.26		1.5 (1.6)	1.4 (1.6)	1.5 (1.6)	1.5 (1.6)
$C_6H_6^+ + NO$			0.73	0.89	0.93	0.99
$C_6H_6NO^+$			0.27	0.11	0.07	0.01
$O_2^+ + C_6H_6 \rightarrow$ products	12.07		1.4 (1.5)			1.5 (1.5)
$C_6H_6^+ + O_2$			1.00			1.00
$N_4^+ + C_6H_6 \rightarrow$ products	12.9		1.2 (1.3)		1.2 (1.3)	1.2 (1.3)
$C_6H_6^+ + 2N_2$			>0.99		>0.99	>0.99
$O^+ + C_6H_6 \rightarrow$ products	13.62		1.9 (2.0)			2.0 (2.0)
$C_6H_6^+ + O$			1.00			1.00
$Kr^+ (^2P_{3/2}) + C_6H_6 \rightarrow$ products	14.00		1.1 (1.2)		1.1 (1.2)	1.2 (1.2)
$C_6H_6^+ + Kr$			1.00		1.00	1.00
$N^+ + C_6H_6 \rightarrow$ products	14.53		2.0 (2.1)		2.0 (2.1)	2.1 (2.1)
$C_6H_6^+ + N$			0.68		0.63	0.62
$C_6H_5^+ + (NH)$			0.07		0.10	0.11
$C_6H_4^+ + (NH_2)$			0.01		0.02	0.02
$C_5H_4^+ + (HCN + H)$			0.07		0.06	0.05
l-$C_4H_4^+ + (CH_2CN)$			0.02		0.03	0.03
c-$C_4H_4^+ + (CH_2CN)$			0.03		0.03	0.03
c-$C_3H_3^+ + (C_2H_2 + HCN)$			0.12		0.13	0.14
$Kr^+ (^2P_{1/2}) + C_6H_6 \rightarrow$ products	14.66		1.1 (1.2)		1.1 (1.2)	1.2 (1.2)
$C_6H_6^+ + Kr$			0.82		0.60	0.65
$C_6H_5^+ + H + Kr$			0.18		0.40	0.35
$N_2^+ + C_6H_6 \rightarrow$ products	15.58	1.5 (1.6)	1.6 (1.6)	1.5 (1.6)	1.7 (1.6)	1.6 (1.6)
$C_6H_6^+ + N_2$		0.13	0.12	0.11	0.10	0.08
$C_6H_5^+ + H + N_2$		0.28	0.24	0.24	0.24	0.23
$C_6H_4^+ + H_2 + N_2$		0.04	0.04	0.03	0.03	0.04
$C_5H_3^+ + CH_3 + N_2$		0.01	0.02	0.02	0.02	0.04
l-$C_4H_4^+ + C_2H_2 + N_2$		0.32	0.36	0.37	0.37	0.38
c-$C_4H_4^+ + C_2H_2 + N_2$		0.04	0.05	0.05	0.06	0.05
c-$C_3H_3^+ + C_3H_3 + N_2$		0.18	0.17	0.18	0.18	0.18
$Ar^+ + C_6H_6 \rightarrow$ products	15.76		1.3 (1.5)		1.5 (1.5)	1.5 (1.5)
$C_6H_6^+ + Ar$			0.08		0.09	0.09
$C_6H_5^+ + H + Ar$			0.18		0.15	0.18
$C_6H_4^+ + H_2 + Ar$			0.03		0.03	0.03
$C_5H_3^+ + CH_3 + Ar$			0.03		0.03	0.03
l-$C_4H_4^+ + C_2H_2 + Ar$			0.48		0.51	0.52
c-$C_4H_4^+ + C_2H_2 + Ar$			0.07		0.05	0.03
c-$C_3H_3^+ + C_3H_3 + Ar$			0.13		0.14	0.12
$F^+ + C_6H_6 \rightarrow$ products	17.42		1.6 (1.9)			
$C_6H_6^+ + F$			0.06			
$C_6H_5^+ + (H + F)$			0.12			
$C_6H_4^+ + (H_2 + F)$			0.01			
$C_4H_3F^+ + (C_2H_3)$			0.03			
$C_5H_3^+ + (CH_3 + F)$			0.07			
l-$C_4H_4^+ + (C_2H_2 + F)$			0.24			
c-$C_4H_4^+ + (C_2H_2 + F)$			0.18			
$C_4H_3^+ + (C_2H_3 + F)$			0.09			
$C_4H_2^+ + (C_2H_4 + F)$			0.04			
c-$C_3H_3^+ + (C_3H_3 + F)$			0.16			
$Ne^+ + C_6H_6 \rightarrow$ products	21.56		1.6 (1.8)		1.8 (1.8)	1.8 (1.8)
$C_6H_6^+ + Ne$			0.01		0.01	0.01
$C_6H_5^+ + H + Ne$			0.02		0.01	0.03
$C_6H_4^+ + H_2 + Ne$			0.02		0.02	0.01
$C_5H_3^+ + CH_3 + Ne$			0.02		0.03	0.02
$C_4H_3^+ + (C_2H_3) + Ne$			0.59		0.60	0.58
$C_4H_2^+ + (C_2H_4) + Ne$			0.09		0.13	0.12
c-$C_3H_3^+ + (C_3H_3) + Ne$			0.11		0.11	0.11
$C_2H_3^+ + (C_4H_3) + Ne$			0.07		0.06	0.07
$C_2H_2^+ + (C_4H_4) + Ne$			0.07		0.03	0.05

[a] Collisional rate constants, k_c, and ion recombination energies (RE) are also indicated for each reactant ion.

the result of C_6H_6 pyrolysis, the data indicate there is at most 10% decomposition of the C_6H_6 at 1400 K with O_2 present simultaneously in the flow tube, and it suggests this is an upper limit for the extent of pyrolysis in the high temperature N_2 experiments. There are several other possible explanations for the origin of these product ions, however. Because the energy spread of the reactant ions is significantly broader in the high temperature experiments than in the experiments done at 300 K, the product ion thresholds can occur at a lower average energy. At best, this appears to only partially explain the data since the product branching fractions at the high temperature thresholds are different than they are at the lower temperature thresholds. An interesting possibility is that reactants with a high degree of vibrational energy may behave differently than the 300 K reactants. We cannot rule out any of these possibilities, and the conditions required to make these measurements

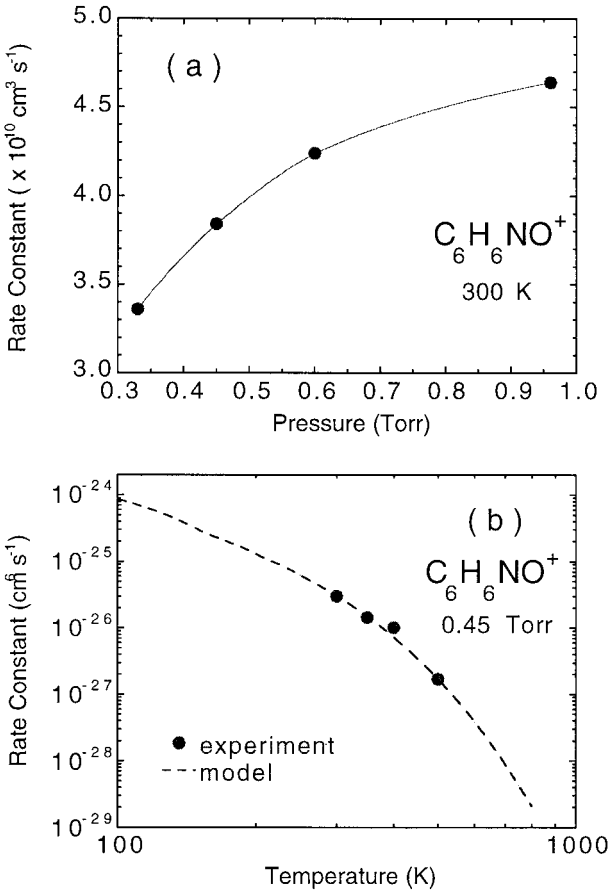

Figure 1. (a) Pressure dependence of the bimolecular rate constant for the $C_6H_6NO^+$ reaction channel at 300 K from 0.33 to 0.96 Torr. (b) Temperature dependence of the three-body association rate constant for NO^+ reacting with C_6H_6 from 300 to 500 K at a pressure of 0.45 Torr. The dashed curve represents the expected temperature dependence of the association reaction based on a model applicable to the low-pressure limit.[22]

TABLE 2: Temperature Dependent Bimolecular Rate Constants and Product Branching Fractions, as Measured with the HTFA from 500 to 1400 K, for the Reaction of Benzene with O_2^+ [a]

	rate constant (10^{-9} cm^3 s^{-1}), (k_c) branching fractions				
	500 K	800 K	1000 K	1200 K	1400 K
$O_2^+ + C_6H_6 \rightarrow$ products	1.3 (1.5)	1.5 (1.5)	1.5 (1.5)	1.6 (1.5)	1.5 (1.5)
$C_6H_6^+ + O_2$	1.00	0.97	0.96	0.93	0.91
$C_6H_5^+ + H + O_2$				0.02	0.02
$C_4H_4^+ + C_2H_2 + O_2$		0.01	0.01	0.01	0.02
$C_4H_3^+ + C_2H_3 + O_2$		0.01	0.02	0.03	0.03
$C_4H_2^+ + C_2H_4 + O_2$		0.01	0.01	0.01	0.02
reactant internal energy (eV)	0.24	0.73	1.15	1.62	2.14

[a] The collisional rate constant, k_c, and the reactant internal plus translational energy are also indicated for each temperature studied.

do not allow for a pressure dependence study in order to further investigate these possibilities. However, we can rule out the possibility that these product ions result from the reaction of benzene with a high energy reactive species, such as helium metastables, since large amounts of O_2 source gas were added, effectively quenching any high energy impurities.[24]

$Kr^+(^2P_{1/2})$ Reaction. It was possible to determine product branching fractions for $Kr^+(^2P_{1/2})$ reacting with benzene by (1) assuming that a statistical mixture of spin−orbit states was produced when Kr^+ was formed via electron impact on Kr[11] and (2) independently studying the reactivity of the $Kr^+(^2P_{3/2})$ state as described above. Unlike the lower spin−orbit state reactant, the $Kr^+(^2P_{1/2})$ reactant yields two product ions, $C_6H_6^+$ and $C_6H_5^+$. The branching fractions for these two product channels change dramatically from 300 to 500 K. The error associated with determining these particular branching fractions is larger than the errors reported for the other VT-SIFT measurements because of our assumption regarding a statistical mixture of spin states being formed. Measurements taken using a statistical mixture of Kr^+ states show only one exponential decay in the parent ion signal, indicating the rate constants for both Kr^+ reactants are equal.

N^+, N_2^+, Ar^+, F^+, and Ne^+ Reactions. The reactions of benzene with N^+, N_2^+, Ar^+, F^+, and Ne^+ all proceed at the collisional rate, with each reactant yielding numerous product ions. As the recombination energy of the reactant ion increases, the $C_6H_6^+$ branching fraction decreases, and $C_6H_5^+$, $C_4H_4^+$, and $C_3H_3^+$ become the major product channels. Minor channels of $C_6H_4^+$ and $C_5H_n^+$ are also observed for each reactant. The $C_5H_n^+$ product is $C_5H_3^+$ for all reactant ions except N^+, which yields a $C_5H_4^+$ product instead. The very energetic reactions of F^+ and Ne^+ yield additional $C_4H_n^+$ products, and Ne^+ also yields $C_2H_n^+$ products.

For the $C_3H_3^+$ and $C_4H_4^+$ products, it was possible to distinguish between cyclic and linear isomers of each species by further examining the reactivity of these product ions with several organic molecules. Previous studies have shown that both isomers of $C_3H_3^+$ react with C_2H_2 and associate with CO; however, in both cases, the cyclic isomer reacts at least 100 times slower than the linear isomer. [25,26] We measured rate constants of 2.4×10^{-12} cm^3 s^{-1} for the reaction of $C_3H_3^+$ with C_2H_2 and 3.2×10^{-29} cm^6 s^{-1} for the association reaction of $C_3H_3^+$ with CO, both rates consistent with this being the cyclic isomer of $C_3H_3^+$. To distinguish the cyclic and linear isomers of $C_4H_4^+$, we followed to completion the secondary chemistry of $C_4H_4^+$ with benzene using long reaction times and large flows of benzene reactant. On the basis of thermodynamic considerations, the reactive isomer is reported to be the vinyl acetylene ion while the unreactive isomer is the methylene cyclopropene ion.[27] Because charge transfer to C_6H_6 is allowed only for the linear isomer, the unreactive component of $C_4H_4^+$ could be attributed to the cyclic isomer. The isomeric mixture was determined for all VT-SIFT measurements (the N^+ and Ar^+ reactions from 300 to 500 K, the N_2^+ reaction from 250 to 500 K, and the F^+ reaction at 300 K) and for one HTFA measurement (the N_2^+ reaction at 1100 K). Our measurements indicate the cyclic isomer is a minor channel, with a branching fraction of 0.02−0.07, for all reactions except F^+, where the branching fraction is dramatically higher at 0.19. Although it is a minor product of the N^+ reaction, the linear isomer of $C_4H_4^+$ is the most abundant product channel for the N_2^+, Ar^+, and F^+ reactions. Compared to the N_2^+ and Ar^+ reactions, the F^+ reaction shows a significant decrease in the linear $C_4H_4^+$ branching fraction.

For the minor $C_5H_3^+$ product ion, it is also possible to have cyclic or linear isomers. The cyclic isomer, the ethynyl cyclopropene ion, is calculated to be the most stable form of $C_5H_3^+$, [28] and it is structurally similar to c-$C_4H_4^+$, while the linear isomers of $C_5H_3^+$, $CH_2{=}C{=}C{-}C{\equiv}CH^+$ and $CH{\equiv}C{-}CH{-}C{\equiv}CH^+$ are structurally similar to linear $C_4H_4^+$. Although the reactivity of these different isomers with benzene has not been reported previously, the similarity of the cyclic and linear isomers of $C_5H_3^+$ and $C_4H_4^+$ suggests cyclic $C_5H_3^+$ will be unreactive toward benzene, while the linear isomers should react readily. In the present study, the $C_5H_3^+$ isomer was found to

TABLE 3: Temperature Dependent Bimolecular Rate Constants and Product Branching Fractions, as Measured with the HTFA from 500 to 1400 K, for the Reaction of Benzene with N_2^+ [a]

	rate constant (10^{-9} cm^3 s^{-1}), (k_c) branching fractions			
	500 K	800 K	1100 K	1400 K
$N_2^+ + C_6H_6 \rightarrow$ products	1.6 (1.6)	1.4 (1.6)	1.6 (1.6)	1.7 (1.6)
$C_6H_6^+ + N_2$	0.06	0.08	0.07	0.11
$C_6H_5^+ + H + N_2$	0.19	0.21	0.22	0.20
$C_6H_4^+ + H_2 + N_2$	0.06	0.04	0.04	0.03
$C_5H_3^+ + CH_3 + N_2$	0.04	0.05	0.06	0.08
$C_4H_4^+ + C_2H_2 + N_2$	0.47	0.45	0.42	0.31
$C_4H_3^+ + (C_2H_3) + N_2$		0.01	0.02	0.08
$C_4H_2^+ + (C_2H_4) + N_2$		0.01	0.02	0.05
$C_3H_3^+ + C_3H_3 + N_2$	0.18	0.15	0.15	0.14
reactant internal energy (eV)	0.24	0.73	1.36	2.14

[a] The collisional rate constant, k_c, and the reactant internal plus translational energy are also indicated for each temperature studied.

be unreactive toward benzene, indicating it is likely that the cyclic isomer is being formed.

The temperature dependence of the N_2^+ reaction was examined from 250 to 500 K in the VT-SIFT and from 500 to 1400 K in the HTFA. Reaction rate constants and product branching fractions measured in the HTFA are shown in Table 3. At 500 K, there is good agreement between the HTFA and VT-SIFT data. From 250 to 1400 K, the reaction rates are independent of temperature; they remain at the collisional value. However, there is a slight temperature dependence of the product branching fractions over this extended temperature range. Branching fractions for the $C_6H_n^+$ and $C_3H_n^+$ channels decrease by about 25%, while the overall $C_4H_n^+$ branching fraction increases by 25% and the $C_5H_3^+$ branching fraction increases from 0.01 to 0.08. Most of this temperature dependence occurs between 250 and 800 K. Above 800 K, the only significant changes that occur are that $C_4H_3^+$ and $C_4H_2^+$ product channels are observed, and their branching fractions increase as the branching fraction of $C_4H_4^+$ decreases. Clearly, the products observed at high temperature do not result primarily from pyrolysis of the benzene reactant. The O_2^+ data indicate that less than 10% of the products observed at 1400 K could result from pyrolysis.

The reactions of N^+ with benzene may involve more than dissociative and nondissociative charge transfer processes, i.e., there may be "reactive" channels as well. In particular, the product ion at m/q of 64 must be the result of a reactive channel since the dissociative charge transfer reaction to yield the lowest energy acyclic isomer of $C_5H_4^+$ (m/q of 64) is significantly endothermic:

$$N^+ + C_6H_6 \rightarrow C_5H_4^+ + CH_2 + N \quad \Delta H = +223 \text{ kJ mol}^{-1} \tag{1}$$

The large endothermicity of reaction 1 suggests the ionic and/or neutral products are not as indicated and leaves open the possibility that this is a reactive channel where the N atom has been incorporated into either the ionic or neutral products. Using $^{15}N^+$ reactant ions, we were able to establish that the ionic product contains only carbon and hydrogen atoms, allowing for the assignment of $C_5H_4^+$. Thus, although we do not characterize the neutral products of these reactions, they appear to involve the formation of a C−N bond, e.g.,

$$N^+ + C_6H_6 \rightarrow C_5H_4^+ + HCN + H \quad \Delta H = -287 \text{ kJ mol}^{-1} \tag{2}$$

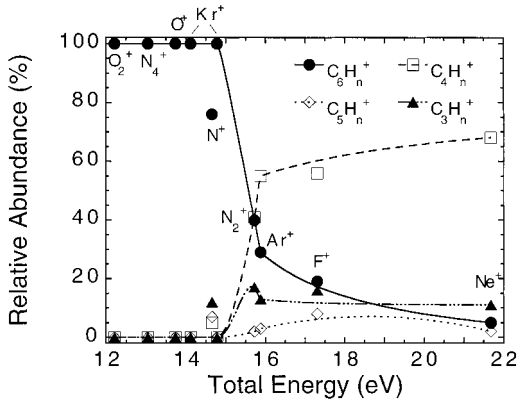

Figure 2. Simplified breakdown diagram of benzene as obtained from data in Table 1. For clarity, only 300 K data are included and products differing by one or two hydrogen atoms are grouped together. Total energy represents the sum of the ion recombination energy and the internal and translational energy of the reactants. Curves are interpolated through all data except that of the N^+ and F^+ measurements.

Further experiments with $^{15}N^+$ confirmed that product ions of the N^+ reaction occurring at m/q of 52 and 39 are $C_3H_3^+$ and $C_4H_4^+$, respectively. For these and the $C_6H_5^+$ and $C_6H_4^+$ product channels, it is not necessary to invoke C−N or H−N bond formation in the neutral products as the dissociative charge transfer reactions are sufficiently exothermic, yet it remains a distinct possibility. As will be shown below, product branching fractions for the N^+ reaction are distinctly different from the other ion reactions studied, suggesting the reaction of N^+ with C_6H_6 may involve reactive and charge transfer mechanisms.

As far as other reactant ions are concerned, the data shown in Table 1 indicate that there are no reactive channels for O_2^+, N_4^+, O^+, and $Kr^+(^2P_{3/2})$ reactions. In addition, reactive channels seem unlikely for N_2^+ and the rare gas cations, Kr^+, Ar^+, and Ne^+. One might expect to have reactive channels with F^+ reactants, and in fact, there is at least one product ion that results from something other than charge transfer. A minor channel yielding $C_4H_3F^+$ was observed. For these reasons, the neutral products of the N^+ and F^+ reactions are listed in parentheses in Table 1, indicating that these products are assumed based on energy arguments.

Discussion

Product Ion Breakdown Curves. A plot of the parent and various product ion branching fractions as a function of energy constitutes the breakdown diagram for a particular compound. For benzene, the breakdown diagram was first determined by Jonsson and Lindholm[1] using charge exchange mass spectrometry and later by Eland et al.[2] using the photoelectron−photoion coincidence technique. At energies below 18 eV, both results indicate there are four primary dissociation products for $C_6H_6^+$: $C_6H_5^+$, $C_6H_4^+$, $C_4H_4^+$, and $C_3H_3^+$. The current flow tube studies of benzene reactions also yield a breakdown diagram for the benzene cation. Simplified breakdown curves for $C_6H_n^+$, $C_5H_n^+$, $C_4H_n^+$, and $C_3H_n^+$ products are shown in Figure 2. For clarity, only the 300 K data are shown, and similar products are grouped together, i.e., those differing by one or two hydrogen atoms. The energy scale represents the sum of the ion recombination energy and the internal and translational energy of the reactants. Reactant zero point energies are not included in this energy. Plotted this way, the 300 K data for O_2^+ appear at 12.2 eV, the N_2^+ data at 15.7 eV, and the Ne^+ data at 21.7 eV. Solid and dashed curves in Figure 2 represent

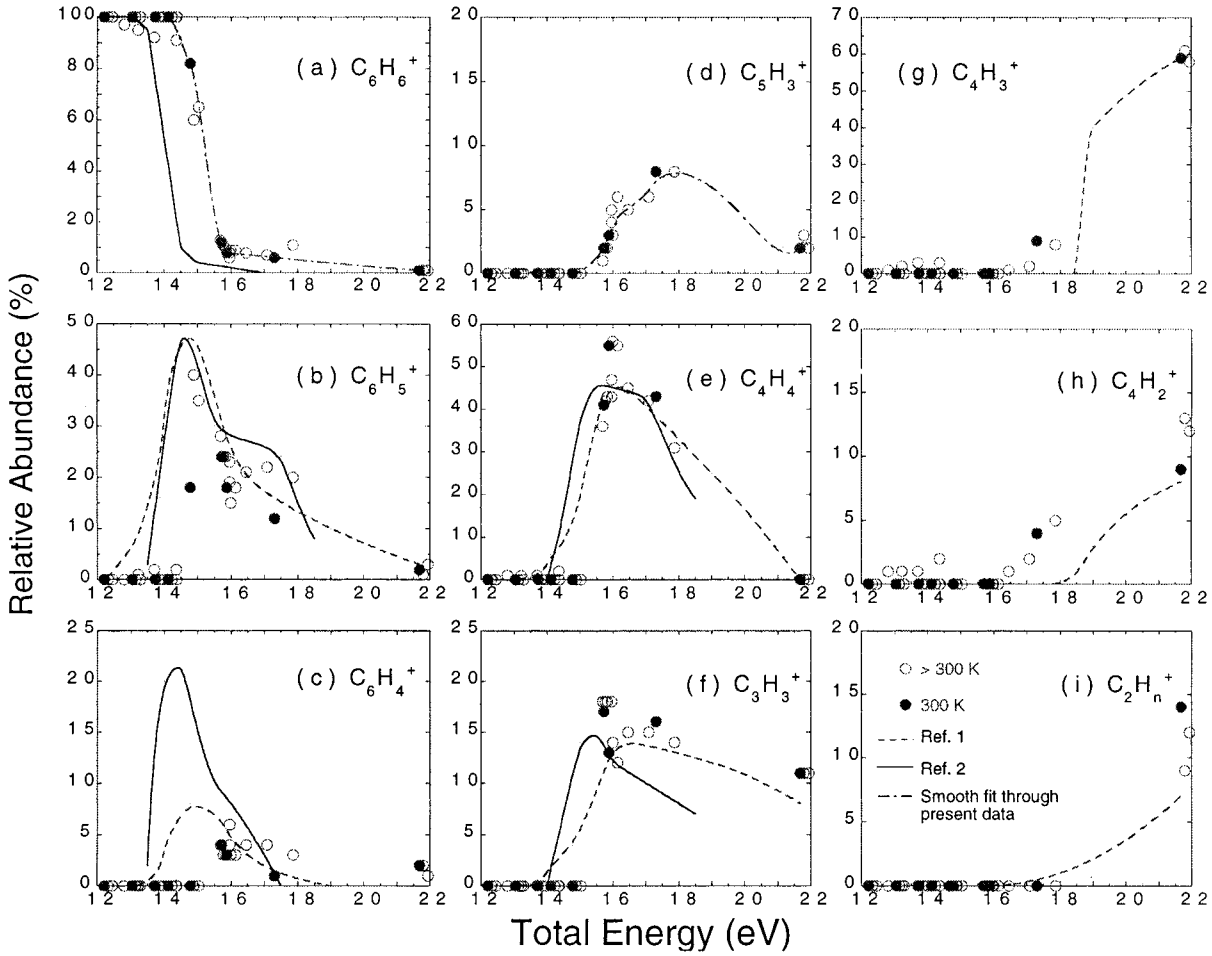

Figure 3. Breakdown curves for each product channel observed in the benzene charge transfer reactions. Solid circles are 300 K SIFT data. Open circles are all other temperature data from the VT-SIFT and the HTFA. The N^+ data have been excluded from the breakdown curves. Solid lines represent breakdown curves obtained previously by the photoelectron−photoion coincidence technique.[2] Dashed lines represent previous charge transfer mass spectral breakdown curves.[1] The reactant internal and translational energies have been added to the energy scale of both the photodissociation and the previous charge transfer mass spectral data. (a) $C_6H_6^+$. Dashed−dotted line is an interpolation through the 300 K SIFT data. Because the photodissociation and the previous charge transfer mass spectral data are essentially identical, only one set of previous data is shown for this channel. (b) $C_6H_5^+$. (c) $C_6H_4^+$. (d) $C_5H_3^+$. Dashed−dotted line is a smooth fit through all flow tube data. There are no previous data for comparison. (e) $C_4H_4^+$. (f) $C_3H_3^+$. (g) $C_4H_3^+$. (h) $C_4H_2^+$. (i) $C_2H_n^+$.

an interpolation through all of the data for each set of products excluding those from N^+ and F^+ reactants; the N^+ and F^+ data may not be a true representation of the breakdown curves because of the reactive product channels that were observed. This simplified breakdown diagram illustrates that (1) the product distribution changes rapidly between 14.5 and 16 eV, as $C_6H_n^+$ decreases and all other product ions increase, (2) there is relatively little change in the product distribution above 17 eV, and (3) $C_4H_n^+$ are the dominant product ions above 15.5 eV. All of this is consistent with the previously determined breakdown diagrams of benzene. However, Figure 2 also demonstrates how the relative product abundances for N^+ (total energy of 14.65 eV) are significantly different compared to $Kr^+(^2P_{3/2})$ and $Kr^+(^2P_{1/2})$ reactant ions (total energies of 14.12 and 14.78 eV, respectively). The N^+ reaction yields less $C_6H_n^+$ and more $C_5H_n^+$, $C_4H_n^+$, and $C_3H_n^+$ products compared to the Kr^+ charge transfer reactions. Most likely, these product ions result from reactive channels and are not due solely to dissociative charge transfer. In contrast, relative product abundances for the F^+ reaction (total energy of 17.31 eV) appear to be only slightly different from what is expected for a purely charge transfer reaction. This could be simply fortuitous, or it could be an indication that the F^+ reactions occur primarily via charge transfer.

Breakdown curves for each individual product channel are shown in Figure 3. In this case, all of the temperature dependent data have been included. To distinguish the various reactant ions, the 300 K data are represented as closed circles and all other temperature data from the VT-SIFT and the HTFA are represented as open circles. The breakdown curves previously reported by Jonsson and Lindholm[1] and by Eland et al.[2] are also included for each channel in Figure 3 as dashed and solid lines, respectively. Relative product ion abundances from the N^+ reaction are not included in Figure 3 since it appears N^+ involves many noncharge transfer processes. In contrast, relative product ion abundances from the F^+ reaction have been included since it remains unclear at this time how important the reactive channel(s) are relative to the charge transfer channels.

As demonstrated in Figure 3a, the relative abundance of the $C_6H_6^+$ parent ion decreases sharply above 14.5 eV. An interpolation through the 300 K SIFT data shows that the VT-SIFT and HTFA data for this product channel generally fall on the same smooth curve. The notable exception is in the energy range from 12.1 to 14.2 eV, where the relative abundance of $C_6H_6^+$ is already decreasing in the HTFA data while it remains at 100% in the VT-SIFT data. As mentioned previously, this difference could be due to C_6H_6 pyrolysis, a broadening of the reactant energy at high temperatures, or different reactivity of

vibrationally excited reactants. There is also a slight deviation from the curve for the highest temperature N_2^+ data at 17.8 eV. However, it should be noted that the determination of the branching fractions at 1400 K required relatively large corrections because of the intense K^+ signal that is also observed at that temperature.

The flow tube data reproduce the trend observed in the earlier breakdown curves except that there is a shift in the threshold energy of approximately 1 eV. This is due in part to a kinetic shift, resulting from slow fragmentation of the energized $C_6H_6^+$*, and also to a pressure effect whereby $C_6H_6^+$* is stabilized via collisions with the He buffer gas. To estimate the magnitude of the expected threshold energy shift in the present experiment, we formulate a simple kinetic model which allows collisional stabilization of the $C_6H_6^+$* to occur, in competition with unimolecular dissociation and radiative relaxation. Rate constants for these processes are given by k_Q, k_{uni}, and k_{rad}, respectively. The total unimolecular dissociation rate, k_{uni}, represents the sum of the individual product channel dissociation rates, $k_1 + k_2 + ... + k_n$. Equation 3 gives the fraction of $C_6H_6^+$ detected relative to the amount of excited $C_6H_6^+$* initially formed:

$$\frac{[C_6H_6^+]}{[C_6H_6^+*]_0} = e^{-(k_{uni} + k_{rad} + k_Q[M])\tau} + \frac{k_{uni} + k_Q[M]}{k_{uni} + k_{rad} + k_Q[M]}[1 - e^{-(k_{uni} + k_{rad} + k_Q[M])\tau}] \quad (3)$$

Using eq 3 and the internal energy selected unimolecular decay rates reported by Kuhlewind et al.,[29] a threshold energy shift, defined as the energy required for ~10% fragmentation in competition with radiative relaxation and collisional quenching of the excited ion,[30] can be estimated. Klippenstein et al.[31] have suggested a value of 700 s^{-1} for k_{rad}; an upper limit for k_Q of 5.4×10^{-10} cm^3 s^{-1} is given by the Langevin collision rate; helium number densities, [M], in the flow tube are approximately 1×10^{16} molecules cm^{-3}, and the reaction time, τ, is approximately 3 ms. To observe a 10% decrease in $[C_6H_6^+*]_0$ in our apparatus, k_{uni} must be approximately 5×10^6 s^{-1}. Comparing this value to the unimolecular decay rates reported by Kuhlewind et al.[29] indicates that the dissociating benzene cations will have internal energies of approximately 5.5 eV. Thus, given that the ionization potential of benzene is 9.25 eV, the expected dissociation energy threshold in our apparatus should be approximately 14.7 eV, which is reasonably close to the threshold we observe. For this reason we conclude that the difference between the energy thresholds in the different experimental methods, as shown in Figure 3, is due to a kinetic shift, resulting from slow fragmentation of the energized $C_6H_6^+$* complex, and to collisional stabilization by the He buffer gas. Interestingly, the correlation between the experimental data and the simple kinetic model detailed in eq 3 implies that the collisional quenching rate, k_Q, of the helium buffer gas is nearly equal to the Langevin rate. This is somewhat surprising given that (1) previous work on ion−molecule association reactions has suggested that the helium buffer gas quenching rate is considerably smaller than the collision rate,[13,32] and (2) a similar analysis of naphthalene flow tube reaction data indicates the buffer gas quenching rate is 5−10 times smaller than the Langevin rate.[8] However, if the collisional quenching rate in the benzene experiments is assumed to be 5−10 times smaller than the Langevin rate, the above analysis would indicate thresholds of 14.4−14.6 eV, which are only slightly lower than what is observed, meaning the analysis is not particularly sensitive to the value of k_Q in this energy region.

The first dissociative charge transfer product ion to be observed in the present experiment is $C_6H_5^+$, at a threshold energy of approximately 14.5 eV. Relative to the previous photodissociation[2] and charge transfer mass spectral data[1] there is a threshold energy shift of approximately 0.9 eV due to the quenching of the excited complex. The temperature dependent flow tube data clearly show the sharp energy dependence of this particular product channel from 14.5 to 16 eV. However, in the region from 16 to 18 eV, where the photodissociation data indicate little energy dependence exists, a significant difference arises between the VT-SIFT and HTFA data. The HTFA data show essentially no temperature dependence in that energy region, while the VT-SIFT data at 300 K (the closed points) appear to decrease smoothly from 15.5 to 21.7 eV. It is possible that this difference is simply an artifact of the F^+ reaction, represented by the data point at total energy of 17.3 eV. Alternatively, this deviation could indicate that $C_6H_6^+$* formed from reactions of C_6H_6 at 300 K is distinct from $C_6H_6^+$* formed with the same excess energy but where a significant portion of the energy is acquired through internal excitation. A difference between the two types of energy is only likely if the IVR rates become slower than the dissociation rate. Unfortunately, this energy range is well beyond the energy range for which dissociation rates have been calculated. Because the photodissociation data demonstrate that the $C_6H_5^+$ breakdown curve is essentially independent of energy in this region, a broadening of the reactant ion energy is unlikely to affect the flow tube data.

At a threshold energy of approximately 15 eV, three additional product ions are observed: $C_6H_4^+$, $C_4H_4^+$, and $C_3H_3^+$. Along with $C_6H_5^+$, these are the major primary dissociation products from $C_6H_6^+$. Although $C_6H_4^+$ is a major product channel from 14 to 15 eV in the previous photodissociation study,[2] it is a minor channel at all energies in the charge transfer mass spectral[1] and flow tube studies. The appearance potential of $C_6H_4^+$ in the photodissociation measurement is essentially the same as that of $C_6H_5^+$, yet the threshold energy shift observed in the flow tube measurements (~ 2 eV) is much larger for $C_6H_4^+$ compared to the other channels. This is even true taking into account the fact that the kinetic shift and the collisional stabilization are suppressing the $C_6H_4^+$ signal in that energy range. The relative abundances of $C_4H_4^+$ and $C_3H_3^+$ from the flow tube measurements compare well with the previous data.[1,2] Relative to the photodissociation results, the flow tube data have a threshold energy shift of approximately 0.8−0.9 eV. Note that for $C_4H_4^+$ and $C_3H_3^+$ channels, the F^+ data (at total energy of 17.31 eV) agree fairly well with the N_2^+ HTFA data taken in that energy region, indicating these products are largely unaffected by possible reactive channels or internal energy effects.

The linear and cyclic isomers of $C_4H_4^+$ have been quantified for various reactants as described previously. These results are shown in Figure 4, along with earlier determinations by Ausloos[27] and by Bowers et al.[33,34] The previous studies have demonstrated that the percentage of reactive linear isomer formed from $C_6H_6^+$ dissociation is a strong function of the parent ion internal energy; in the threshold region, the more stable cyclic isomer is formed exclusively, but the linear isomer is accessible and eventually becomes the dominant channel above 15.6 eV. Using the charge transfer reaction between $C_4H_4^+$ and benzene to titrate the isomeric mixture, Ausloos reported that $C_4H_4^+$ ions formed at threshold almost exclusively

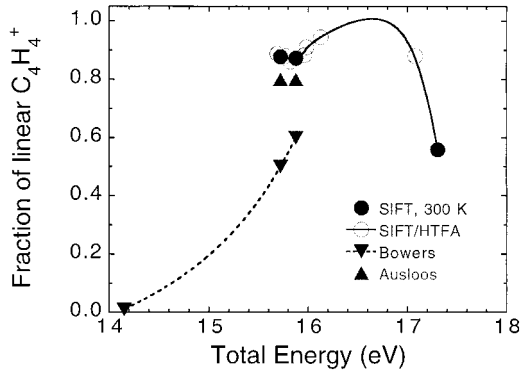

Figure 4. Fraction of linear $C_4H_4^+$ formed from benzene charge transfer reactions as a function of energy. Solid circles are 300 K SIFT data. Open circles are all other temperature data from the VT-SIFT and the HTFA. Previous results by Ausloos[27] and by Bowers et al.[34] are also shown.

have the cyclic structure, while 80% of the ions formed at 2 eV higher in energy have the linear structure. Bowers et al. have also determined the isomeric mixture of $C_4H_4^+$ ions formed at that energy by examining the ratio of particular ions in the $C_4H_4^+$ CID fragmentation pattern. Because this is a more indirect determination, the authors caution that the uncertainty in their experimental values is rather large. However, they have also calculated the isomeric mixture expected at energies from threshold up to ~2 eV higher in energy using statistical rate theory, and the calculated values are similar to their experimental measurements. The calculated values are shown in Figure 4. The flow tube data are in good agreement with the results of Ausloos, while the combined experimental and theoretical results of Bowers et al. consistently yield a smaller percentage of linear $C_4H_4^+$. At higher energies, the flow tube data indicate that the percentage of linear isomer formed from $C_6H_6^+$ dissociation again decreases. Unfortunately, that conclusion is based primarily on the value at 17.3 eV, which represents the F^+ reaction with benzene. Although the total $C_4H_4^+$ branching fraction from the F^+ reaction was consistent with the other charge transfer results (see Figure 3e), we cannot rule out the possibility that this significant change in the isomeric mixture is simply an artifact of the F^+ reaction.

Assuming the behavior we observe is not an artifact of the F^+ reaction but actually results from the charge transfer process, the data shown in Figure 4 may indicate that another unreactive $C_4H_4^+$ product channel such as cyclobutadiene becomes accessible in that energy range. However, this seems unlikely given the ab initio calculations of van der Hart.[35] In examining the four classical $C_4H_4^+$ structures (methylene cyclopropene, vinyl acetylene, cyclobutadiene, and butatriene) and their possible fragmentation pathways from $C_6H_6^+$, van der Hart found the methylene cyclopropene isomer is the dissociation path of lowest energy, while the barriers and the energies of the separated fragments for the other three structures are very similar. As for the experimental observation that only vinyl acetylene is formed, van der Hart attributes this to the fact that the transition states for vinyl acetylene formation are more similar to the benzene structure than they are to the transition states for the other classical structures.

The data obtained for the N^+ reaction are not included in Figure 4 because the reaction appears to yield product ions below the charge transfer threshold, a further indication of reactive channels being present. Nevertheless, we were able to quantify the isomeric mixture for the N^+ reaction as well, showing that nearly equal amounts of cyclic and linear $C_4H_4^+$ isomers were formed.

In addition to the product channels discussed above, the flow tube experiments yield several product ions at higher energy thresholds. At approximately 15.5 eV, $C_5H_3^+$ is observed. It is always a relatively minor product, smoothly increasing to near 10% relative abundance and then decreasing again at very high energies. This product channel was not reported in the previous breakdown diagrams for benzene. However, previous metastable ion fragmentation and collision-induced dissociation studies,[36,37] which have elucidated many of the fragmentation pathways of the benzene cation, indicate that $C_5H_3^+$ is indeed a primary, although minor, dissociation pathway of $C_6H_6^+$. Assuming the threshold energy shift for $C_5H_3^+$ is similar to that of the other primary products, the real appearance potential of this product should be about 14.8 eV. At approximately 16 eV, $C_4H_3^+$ and $C_4H_2^+$ products are observed, with $C_4H_3^+$ becoming the dominant product channel above 19 eV. Both of these products are secondary fragments; $C_4H_3^+$ results from $C_4H_4^+$ and $C_6H_5^+$ dissociation, while $C_4H_2^+$ results from dissociation of $C_4H_3^+$, $C_4H_4^+$, and $C_6H_4^+$. These channels were also observed by Jonsson and Lindholm,[1] but they were not reported by Eland et al.[2] The difference between our data and that of Jonsson and Lindholm results from the fact that they did not probe the threshold region; they used the appearance potentials for $C_4H_3^+$ and $C_4H_2^+$ obtained from electron impact (~18.4 eV) to set the threshold energies for these channels. Generally, appearance potentials reported from electron impact studies are higher than ones reported from photoionization.[3] Finally, at even higher energies, $C_2H_n^+$ products are observed, with a combined relative abundance of nearly 15% at 22 eV. Jonsson and Lindholm also observed these product ions at high energy, with ~7% $C_2H_n^+$ products at ~22 eV. Interestingly, the metastable ion fragmentation and CID studies of $C_6H_6^+$ reveal no processes that yield $C_2H_2^+$ or $C_2H_3^+$ ions from singly charged $C_6H_6^+$. However, formation of $C_2H_3^+$ from decomposition of the doubly charged ion, $C_6H_5^{2+}$ has been reported. Given the energy required, this doubly charged cation mechanism is not possible in the flow tube experiment. [28]

Primary Fragmentation Channels of $C_6H_6^+$. The determination of structures for the four primary fragment ions of benzene is discussed in detail in the review article by Rosenstock et al.[3] Briefly, thermochemical evidence indicates the $C_6H_5^+$ product has the phenyl ion structure; the $C_6H_4^+$ product is thought to be an isomer of the benzyne ion, probably 1,2 benzyne; the $C_4H_4^+$ product is reported to be the cyclic isomer (methylene cyclopropene) at threshold energies and a mixture of cyclic and linear isomers (vinyl acetylene) at higher energies; and the $C_3H_3^+$ product is believed to be the cyclopropenyl ion. Although the structure of the minor primary fragment, $C_5H_3^+$, has not been firmly established, the current flow tube data suggest it is the low energy cyclic ethynyl cyclopropenyl isomer.

On the basis of the photoelectron−photoion coincidence (PEPICO) results of Baer et al.,[38] the multiphoton ionization results of Kuehlewind et al.,[29] and the combined experimental and theoretical studies of Jarrold et al. [34] and Klippenstein et al.,[31] it is now well established that, up to ~16 eV, the four primary $C_6H_6^+$ dissociation reactions are all in competition with each other and are well described by statistical theories. The $C_6H_5^+$, $C_6H_4^+$, $C_4H_4^+$, and $C_3H_3^+$ fragment ions were shown to originate from a common energized complex, the ground electronic state of $C_6H_6^+$, which is formed via fast internal conversion processes from excited electronic states. The lifetime of the energized complex is quite long, ~1 ms near threshold, and it increases exponentially with increasing ion energy. The decay rate constants for all four channels were found to be in

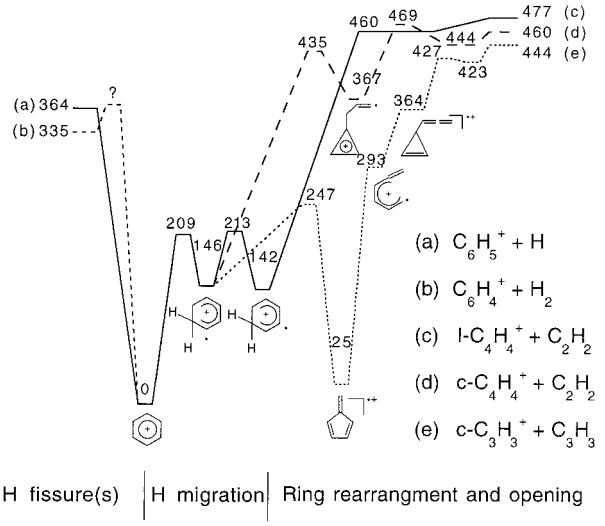

Figure 5. Schematic reaction coordinate diagram of $C_6H_6^+$ dissociation constructed from previous experimental and theoretical results as described in the text. Energies are in kJ/mol. Dissociation limits are obtained from experimental heats of formations.[41] The $C_3H_3^+$ and $C_4H_4^+$ reaction pathways are taken from the ab initio calculations of van der Hart,[35,40] which were performed at the 6-31G** level of theory. Energies along the c-$C_3H_3^+$ and c-$C_4H_4^+$ pathways have been adjusted after the common intermediate to match experimental dissociation limits.

good agreement with RRKM calculations, confirming the statistical character of the $C_6H_6^+$ ion dissociation. Above 16 eV, the dissociation is not well described by statistical theories, possibly because of the dissociation rates becoming comparable to the isomerization rate.

A schematic reaction coordinate diagram representing the four primary dissociation channels of $C_6H_6^+$ has been constructed from previous experimental and theoretical work and is shown in Figure 5. All product channels originate from the ground electronic state of $C_6H_6^+$. For clarity, product channels that involve only H-fissure(s) are shown on one side of the diagram, while product channels that involve H-migration, rearrangement, and then carbon−carbon bond breaking are shown on the opposite side of the diagram.

Dissociation limits for the H-fissure product ions, $C_6H_5^+$ and $C_6H_4^+$, were obtained from experimental heats of formation.[39] Kinetic energy release distributions for both channels, as well as rate constants for the back reactions, have been reported by Jarrold et al.[34] The reaction rate and kinetic energy release distribution for the $C_6H_5^+$ channel are consistent with there being no barrier along the reaction coordinate. However, data for the $C_6H_4^+$ channel suggest that a substantial barrier exists along that coordinate. Since $C_6H_5^+$ is the lowest energy dissociation fragment observed experimentally, the barrier for the ($C_6H_4^+ + H_2$) channel has been drawn slightly higher than the dissociation limit for the ($C_6H_5^+ + H$) channel.

For the $C_3H_3^+$ product channel, the kinetic energy release distribution and the rate constant for the back reaction are characteristic of a reaction with no significant reverse activation barrier.[34] A more detailed picture of the reaction pathway that produces c-$C_3H_3^+$ fragments is provided by the ab initio calculation of van der Hart.[40] The calculation indicates that (1) the highest barrier in the fragmentation pathway is slightly lower than the total energy of the separated fragments, consistent with the results of Jarrold et al.,[34] and (2) the reaction pathway consists of an isomerization of the benzene cation to the fulvene structure, followed by rearrangement to the allyl cyclopropene cation and then loss of linear C_3H_3 neutral. The total energy of the separated fragments was found to be somewhat higher than the experimental value. Better agreement is expected from calculations that utilize a larger basis set; however, it is unlikely to result in an overall different picture of the fragmentation pathway. Thus, to compare all of the fragmentation channels in Figure 5, the calculated energy values along the $C_3H_3^+$ reaction pathway have been adjusted, after the common intermediate, to conform to the experimental dissociation energies. For the ($C_3H_3^+ + C_3H_3$) channel, this required subtracting 25 kJ/mol from the calculated values.

For the $C_4H_4^+$ product channel, both cyclic and linear isomers need to be considered. Experimental and theoretical results indicate that isomerization of $C_4H_4^+$ fragmentation products is very unlikely, meaning the cyclic and linear products result from different isomerizations of $C_6H_6^+$ prior to fragmentation.[35] The results of Jarrold et al. [34] indicate there is no barrier along the reaction pathway for the linear isomer, while there may be a barrier for the cyclic isomer. The ab initio calculations by van der Hart[35] indicate that the lowest energy $C_4H_4^+$ dissociation pathway from the benzene cation is that which forms the methylene cyclopropene ion, i.e., the cyclic isomer. The reaction pathway for c-$C_4H_4^+$ consists of an isomerization of the benzene cation that involves only a H-migration, followed by a higher energy rearrangement to the propylene cyclopropene cation, and then loss of C_2H_2 neutral. Note that the c-$C_4H_4^+$ reaction pathway has a significant high-energy well. The calculated dissociation limits for the c-$C_4H_4^+ + C_2H_2$ channel were 29 kJ/mol lower than the values obtained from experimental heats of formation and were adjusted accordingly in Figure 5 for all points on the reaction pathway after the common intermediate. For the linear $C_4H_4^+$ isomer (the vinyl acetylene ion), the calculated reaction pathway involves a slightly different isomerization of the benzene cation, followed by essentially direct fragmentation of acetylene neutral. The calculated dissociation limit for the linear $C_4H_4^+ + C_2H_2$ channel is in good agreement with the experimental value.

Although not shown in Figure 5, it is likely that the $C_5H_3^+$ product, which is a minor primary dissociation channel, is also in competition with the four main channels. If the ion has the cyclic ethynyl cyclopropene structure as the flow tube results suggest, a likely reaction pathway is one similar to that of c-$C_4H_4^+$: H-migration from the benzene cation, followed by rearrangement to the propylene cyclopropene cation, followed by loss of CH_3 neutral. The dissociation limit for this channel, based on estimated heats of formation[28] for $C_5H_3^+$, is 473 kJ/mol, very similar to the $C_3H_3^+$, c-$C_4H_4^+$, and linear $C_4H_4^+$ channels. As described earlier, the experimental threshold energy for this channel is found to be higher than the thresholds for $C_3H_3^+$ and $C_4H_4^+$, suggesting there is a barrier to forming the $C_5H_3^+$ product.

Pressure Dependence of Product Branching Fractions. Given the threshold energy shifts observed in the flow tube experiments, which are due in part to collisional quenching of the $C_6H_6^{+*}$ precursor, we wanted to explore the pressure dependence of the product branching fractions. To observe an effect, we needed to study the pressure dependence of a reaction where both the dissociative and nondissociative charge transfer branching fractions change rapidly with energy. From Figure 2, we see that this occurs in the energy range from 14.5 to 15.5 eV. The only reaction in this energy range amenable to a pressure dependence study was N^+, which in retrospect is not an ideal choice because it now appears to involve reactive channels as well as the charge transfer channels. The pressure dependence of the N^+ reaction was measured from 0.33 to 0.75 Torr, and the results are shown in Figure 6. The product

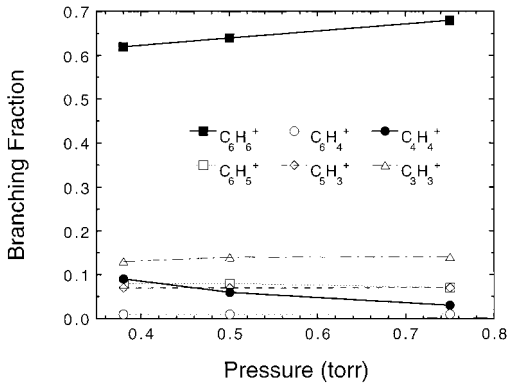

Figure 6. Pressure dependence of the branching fractions for N^+ reacting with C_6H_6 at 300 K from 0.33 to 0.75 Torr. Curves are meant to guide the eye.

branching fractions for this reaction exhibit only a slight pressure dependence over this range; the $C_4H_4^+$ branching fraction decreases with increasing pressure, while $C_6H_6^+$ increases a comparable amount. The $C_6H_5^+$, $C_5H_4^+$, and $C_3H_3^+$ branching fractions are essentially constant over this pressure range.

We attempted to simulate the pressure dependence shown in Figure 6 using the model of $C_6H_6^+$* dissociation described earlier, as well as more complicated models involving intermediates, where the various energized complexes are allowed to undergo radiative relaxation and collisional quenching to generate stable $C_6H_6^+$ products, in competition with unimolecular dissociation to generate the various fragmentation products. To reproduce the pressure dependence shown in Figure 6, we found it was necessary to invoke nonequivalent collisional quenching rates, k_{Qn}, and fragmentation rates, k_n, for the different product channels. For the pressure independent product channels, it was necessary to set k_{Qn} much larger than k_n. Unfortunately, under these conditions, the model yields absolute product branching fractions that do not reproduce the measured values. Alternatively, one could adjust the values of k_{Qn} to reproduce the measured product branching fractions, but this does not reproduce the pressure dependence of the reaction. We conclude that the lack of a pressure dependence in $C_6H_5^+$, $C_5H_3^+$, and $C_3H_3^+$ channels indicates these products are likely formed at least in part by reactive processes and not through dissociative charge transfer. In addition, the fact that there is a pressure dependence in the $C_4H_4^+$ channel indicates that some portion of that product ion results from a unimolecular decay process.

While these results are not completely applicable to the pressure dependence involved in shifting the threshold, they do show that the buffer gas can affect the reactivity. In particular, the increase in the $C_6H_6^+$ channel at the expense of the $C_4H_4^+$ channel may indicate that we are trapping in the high-energy exit well of the $C_4H_4^+$ channel and that the added $C_6H_6^+$ may be an isomeric form. In fact, this is the only channel that has an exit well and indicates that products appear slowly after the rearrangement.

Summary

In this paper, we report kinetics studies of a series of benzene charge transfer reactions, ranging from a reaction that is nearly thermoneutral to one that is over 12 eV exothermic. Temperature dependent rate constants and product branching fractions were determined for all of these reactions, in some cases up to 1400 K. This is one in a series of recent measurements on hydrocarbon reactions from our laboratory, where for the first time branching fractions have been determined for ion−molecule reactions at such high temperatures.

All of the benzene reactions studied proceed at the collisional rate. With increasing reactant ion energy, the mechanism changes from association to nondissociative charge transfer and then to dissociative charge transfer. A total of six primary dissociation products are observed: $C_6H_5^+$, $C_6H_4^+$, $C_5H_3^+$, c-$C_4H_4^+$, linear $C_4H_4^+$, and $C_3H_3^+$. Several secondary dissociation products are also observed: $C_4H_3^+$, $C_4H_2^+$, $C_2H_3^+$, and $C_2H_2^+$.

The temperature dependent branching fractions were converted to product ion breakdown curves. The current results are similar to breakdown curves obtained previously by charge transfer mass spectral and photodissociation studies except that there is a shift in the observed threshold energy which ranges from ~0.7 to 2 eV. The difference in threshold energies is due to a kinetic shift, resulting from slow fragmentation of the $C_6H_6^+$* complex, combined with collisional stabilization of the complex by the He buffer gas.

To explore the effects of collisional quenching on the product branching fractions, the pressure dependence of the N^+ reaction was examined. The measured pressure dependence cannot be explained by assuming that all of the primary reaction channels originate from a common complex and are in competition with one another, as is the case for $C_6H_6^+$ dissociation. It appears the N^+ reaction with benzene is an anomaly in this study, involving many noncharge transfer processes.

In addition to establishing that the $C_3H_3^+$ products are the unreactive cyclic isomer, the isomeric mixture of linear and cyclic $C_4H_4^+$ products has been quantified as a function of the $C_6H_6^+$* excess energy. The cyclic isomer dominates at threshold, and at slightly higher energies the linear isomer becomes the dominant species. These flow tube results are consistent with previous measurements. At higher energies, where no previous data exist for comparison, it appears the linear−cyclic isomeric mixture changes significantly again.

The flow tube data provide the first breakdown curve for the minor primary fragment ion, $C_5H_3^+$. These results also indicate that the $C_5H_3^+$ product is relatively unreactive, consistent with it having the cyclic ethynyl cyclopropene ion structure, analogous to the c-$C_4H_4^+$ product.

A schematic reaction coordinate diagram representing the four primary dissociation channels of $C_6H_6^+$ was constructed from previous experimental and theoretical work. A possible reaction pathway for the minor primary fragment ion, $C_5H_3^+$, was discussed on the basis of the present flow tube results.

Acknowledgment. Technical support from John Williamson and Paul Mundis is gratefully acknowledged. This research was supported by the Air Force Office of Scientific Research under Project No. 2303EP4. A.J.M. is an Air Force Research Laboratory Scholar.

References and Notes

(1) Jonsson, B. O.; Lindholm, E. *Arkiv Fysik* **1967**, *39*, 65.

(2) Eland, J. H. D.; Frey, R.; Schulte, H.; Brehm, B. *Int. J. Mass Spectrom. Ion Phys.* **1976**, *21*, 209.

(3) Rosenstock, H. M.; Dannacher, J.; Liebman, J. F. *Radiat. Phys. Chem.* **1982**, *20*, 7.

(4) Arnold, S. T.; Viggiano, A. A.; Morris, R. A. *J. Phys. Chem. A* **1997**, *101*, 9351.

(5) Arnold, S. T.; Viggiano, A. A.; Morris, R. A. *J. Phys. Chem. A* **1998**, *102*, 8881.

(6) Arnold, S. T.; Morris, R. A.; Viggiano, A. A. *J. Phys. Chem. A* **1998**, *102*, 1345.

(7) Williams, S.; Arnold, S. T.; Morris, R. A.; Maurice, L. Q.; Viggiano, A. A.; Bench, P.; Dotan, I.; Midey, A. J.; Morris, T.; Sutton, E. A. *Potential enhancement of hydrocarbon fueled combustor performance via ionization*; Florence, Italy, 1999.

(8) Midey, A. J.; Williams, S.; Arnold, S. T.; Dotan, I.; Morris, R. A.; Viggiano, A. A. *Int. J. Mass Spectrom.* **1999**, in press.

(9) Dotan, I.; Viggiano, A. A. *J. Am. Chem. Soc.*, submitted for publication.

(10) Praxmarer, C.; Hansel, A.; Lindinger, W.; Herman, Z. *J. Chem. Phys.* **1998**, *109*, 4246.

(11) Viggiano, A. A.; Morris, R. A.; Dale, F.; Paulson, J. F.; Giles, K.; Smith, D.; Su, T. *J. Chem. Phys.* **1990**, *93*, 1149.

(12) Hierl, P. M.; Friedman, J. F.; Miller, T. M.; Dotan, I.; Mendendez-Barreto, M.; Seeley, J.; Williamson, J. S.; Dale, F.; Mundis, P. L.; Morris, R. A.; Paulson, J. F.; Viggiano, A. A. *Rev. Sci. Instrum.* **1996**, *67*, 2142.

(13) Ikezoe, Y.; Matsuoka, S.; Takebe, M.; Viggiano, A. A. *Gas Phase Ion−Molecule Reaction Rate Constants Through 1986*; Maruzen Company, Ltd.: Tokyo, 1987.

(14) Tichy, M.; Rakshit, A. B.; Lister, D. G.; Twiddy, N. D.; Adams, N. G.; Smith, D. *Int. J. Mass Spectrom. Ion Phys.* **1979**, *29*, 231.

(15) Moore, C. E. *Atomic Energy Levels*; National Bureau of Standards: Washington, D.C., 1971.

(16) Ferguson, E. E. *J. Phys. Chem.* **1986**, *90*, 731.

(17) Smith, R. D.; Johnson, A. L. *Combust. Flame* **1983**, *51*, 1.

(18) Gioumousis, G.; Stevenson, D. P. *J. Chem. Phys.* **1958**, *29*, 294.

(19) Su, T.; Chesnavich, W. J. *J. Chem. Phys.* **1982**, *76*, 5183.

(20) Su, T. *J. Chem. Phys.* **1988**, *89*, 5355.

(21) Spanel, P.; Smith, D. *Int. J. Mass Spectrom.* **1998**, *181*, 1.

(22) Viggiano, A. A. *J. Chem. Phys.* **1986**, *84*, 244.

(23) Herzberg, G. *Molecular Spectra and Molecular Structure: II. Infrared and Raman Spectra of Polyatomic Molecules*; D. Van Nostrand Co., Inc.: New York, 1945.

(24) Lindinger, W.; Schmeltekopf, A. L.; Fehsenfeld, F. C. *J. Chem. Phys.* **1974**, *61*, 2890.

(25) Smith, D.; Adams, N. G. *Int. J. Mass Spectrom. Ion Processes* **1987**, *76*, 307.

(26) Smyth, K. C.; Lias, S. G.; Ausloos, P. *Combust. Sci. Technol.* **1982**, *28*, 147.

(27) Ausloos, P. *J. Am. Chem. Soc.* **1981**, *103*, 3931.

(28) Lammertsma, K.; Schleyer, P. v. R. *J. Am. Chem. Soc.* **1983**, *105*, 1049.

(29) Kuhlewind, H.; Kiermeier, A.; Neusser, H. J. *J. Chem. Phys.* **1986**, *85*, 4427.

(30) Lifshitz, C. *Acc. Chem. Res.* **1994**, *27*, 138.

(31) Klippenstein, S. J.; Faulk, J. D.; Dunbar, R. C. *J. Chem. Phys.* **1993**, *98*, 243.

(32) Seeley, J. V.; Morris, R. A.; Viggiano, A. A.; Wang, H.; Hase, W. L. *J. Am. Chem. Soc.* **1997**, *119*, 577.

(33) Wagner-Redeker, W.; Illies, A. J.; Kemper, P. R.; Bowers, M. T. *J. Am. Chem. Soc.* **1983**, *105*, 5719.

(34) Jarrold, M. F.; Wagner-Redeker, W.; Illies, A. J.; Kirchner, N. J.; Bowers, M. T. *Int. J. Mass Spectrom. Ion Processes* **1984**, *58*, 63.

(35) van der Hart, W. J. *Int. J. Mass Spectrom.* **1998**, *176*, 23.

(36) Ottinger, C. *Z. Naturforsch* **1965**, *20a*, 1229.

(37) Jennings, K. R. *Z. Naturforsch* **1967**, *22a*, 454.

(38) Baer, T.; Willett, G. D.; Smith, D.; Phillips, J. S. *J. Chem. Phys.* **1979**, *70*, 4076.

(39) Lias, S. G.; Bartmess, J. E.; Liebman, J. F.; Holmes, J. L.; Levin, R. D.; Mallard, W. G. In *NIST Chemistry WebBook, NIST Standard Reference Database Number 69*; Mallard, W. G., Linstrom, P. J., Eds.; NIST: Gaithersburg, 1998.

(40) van der Hart, W. J. *Int. J. Mass Spectrom. Ion Processes* **1997**, *171*, 269.

(41) Lias, S. G.; Bartmess, J. E.; Liebman, J. F.; Holmes, J. L.; Levin, R. D.; Mallard, W. G. *J. Phys. Chem. Ref. Data* **1988**, *17*, *Supplement 1*, 1.